Combining pressure and electrochemistry to synthesize palladium superhydrides

Pin-Wen Guan[1], Russell J. Hemley[2,3], Venkatasubramanian Viswanathan[1,4]

[1]*Department of Mechanical Engineering, Carnegie Mellon University, Pittsburgh, Pennsylvania 15213, USA*

[2]*Department of Physics, University of Illinois at Chicago, Chicago, IL 60607 USA*

[3]*Department of Chemistry, University of Illinois at Chicago, Chicago, IL 60607 USA*

[4]*Department of Physics, Carnegie Mellon University, Pittsburgh, Pennsylvania 15213, USA*

Palladium-hydrogen is a widely-studied material system with the highest hydride phase being Pd_3H_4. Recently, superhydrides (MH_n with $n > 6$) have been computationally identified and synthesized with rare-earth and early transition metals under pressure. In this work, we evaluate the possibility of electrochemically synthesizing palladium superhydrides together with applied pressure. We perform a computational search for palladium superhydrides using density functional theory calculations and particle swarm optimization over a broad range of pressures and electrode potentials. We incorporate exchange-correlation functional uncertainty using the Bayesian error estimation formalism to quantify the uncertainty associated with the identified stable phases. Based on a thermodynamic analysis, we construct a pressure-potential phase diagram that provides an alternate route to accessing novel Pd-H phases having high hydrogen content. Most strikingly, at potentials above hydrogen evolution and $\sim$200 MPa pressure, we find the possibility to make palladium superhydrides (e.g., PdH_{10}). As palladium is among the most active hydrogen evolution electrocatalysts, a similar strategy is likely to work for electrochemical synthesis of other metal superhydrides at modest pressures.

Palladium-hydrogen system has long attracted research interests due to its importance in both fundamental science and technological applications[1,2]. It has been studied for potential applications in superconductivity[3], hydrogen uptake[4], and low-energy nuclear reactions[5]. Experimentally, the highest hydride phase synthesized is Pd_3H_4[6], under high pressure conditions. There is now great interest in metal hydrides produced under pressure that contain significantly higher amounts of hydrogen, including superhydrides (defined as MH_n, for $n > 6$) first synthesized in the La-H

system[7] as guided by theoretical calculations[8,9].

Here we explore the phase stability of higher hydrides of Pd as a function of pressure and electrochemical conditions (electrode potential, pH) using density-functional theory (DFT)based structure search methods. We also examine the dependence of the results on the choice of exchange correlation functional within the Bayesian error estimation formalism. After a detailed discussion of the identified stable structures, we present a calculated pressure-dependent electrochemical phase diagram of palladium hydride. Based on these calculations, we find an alternate approach to access Pd-H phases having high hydrogen content. Most strikingly, we find that it is thermodynamically feasible to electrochemically synthesize PdH_{10} at a modest pressure of 200 MPa (2 kbar). The stability line of phase boundary between PdH and PdH_{10} shows that three orders of magnitude in pressure could be compensated by a modest electrochemical driving force of $\sim$0.1 V. The results open new opportunities for the creation of metal superhydrides and other novel materials by combining pressure and electrochemical loading techniques.

Structure search and analysis

The phase stability of Pd-H phases over a wide range of compressions was explored using density-functional theory combined with the CALYPSO structure search method[10,11]. To identify the range of stable structures and stoichiometries possible, we initially focused on results obtained at zero pressure and megabar (150 GPa) pressures. The Bayesian error estimation functional with van der Waals correlation (BEEF-vdW) was employed to provide a confidence value (c-value) for compet-

ing phases to avoid possible bias due to selection of a particular DFT functional[12], an approach that has been successfully applied to calculate uncertainty in phase diagrams for other systems[13,14]. To enhance robust assessment of the ground state within the structure search, we used the ensemble of functionals within the BEEF formulation to identify the predicted ground state. Thus, each functional identifies a particular ground state for a given composition and c-value quantifies what fraction of the functionals identify that structure as having the minimum energy.

We begin by discussing the structure search performed for the two experimentally assessed compositions at ambient and high pressure, PdH and Pd_3H_4. For PdH, we find several structures close in energy. We use the Bayesian error estimation capability within BEEF-vdw to construct a confidence-value (c-value) diagram (Fig. 1). This analysis indicates that the most probable predicted ground state of PdH has the $R3m$ space group with Pd in tetrahedral coordination. However, this structure has a c-value of around 0.4, indicating that at GGA-level DFT, it is not possible to conclusively identify the true ground state. We recover the experimentally reported $Fm\bar{3}m$ rocksalt structure as one of the possible structures, though it has a lower c-value (about 0.05). At high pressure (e.g., 150 GPa), the method gives the rocksalt structure as the most probable with a high c-value, indicating that on compression this structure is indeed the ground state predicted at the GGA-level of theory. These results are consistent with experiments reported up to 100 GPa[15,16].

We next consider Pd_3H_4, which is the only higher hydride reported experimentally, e.g., at around 5 GPa[6]. The structure search calculations identify a structure with Pd having 5-fold and 6-fold coordination and space group Cm as the most probable (Fig. S1). We recover the experimen-

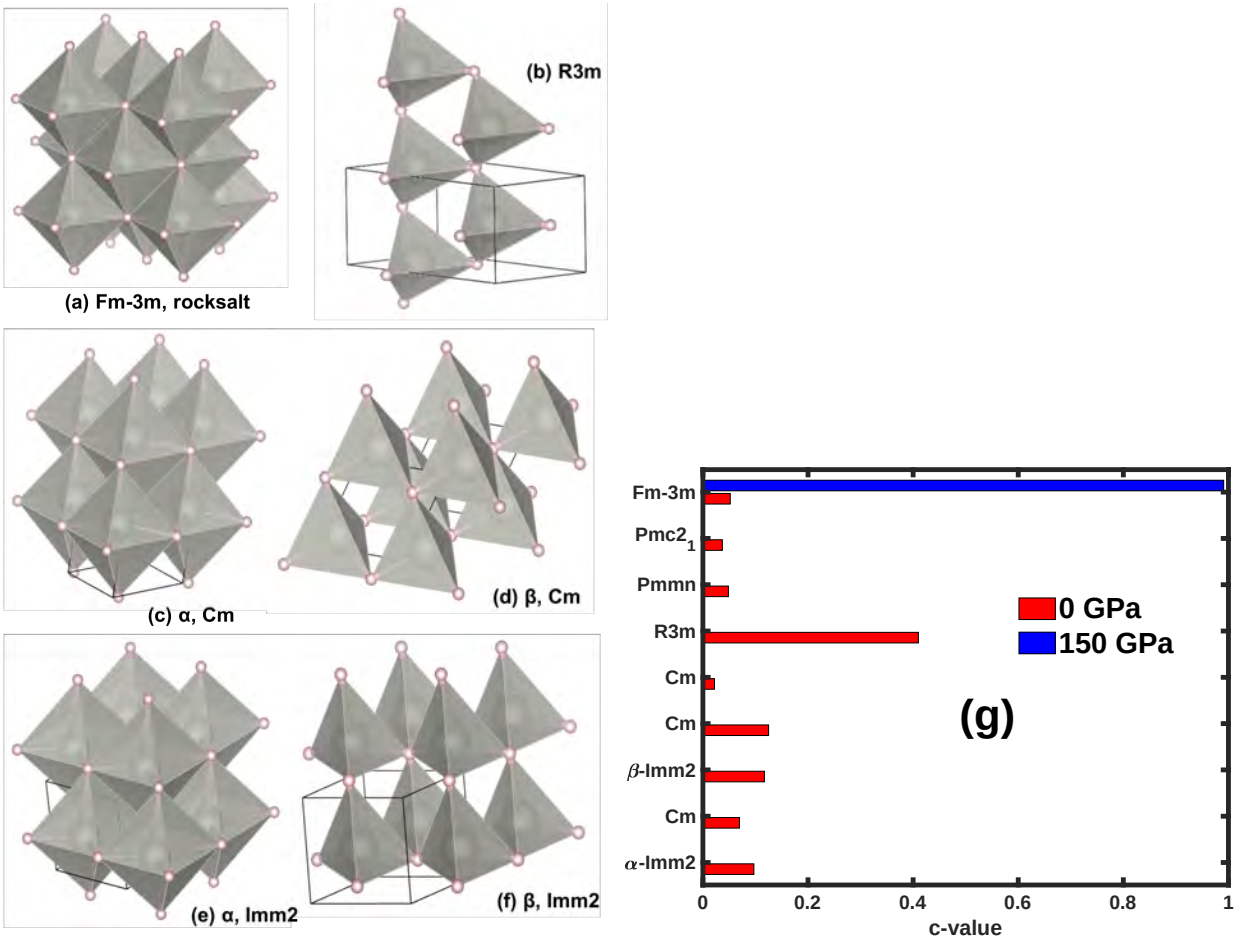

Figure 1: Crystal structures of PdH (a) $Fm\bar{3}m$ and (b) $R3m$. In the $Fm\bar{3}m$ structure, the Pd atom is octahedrally coordinated whereas in $R3m$, Pd is tetrahedrally coordinated. (c) Ground states with c-values of PdH at zero pressure and 150 GPa calculated by BEEF-vdW. The most probable structure has the $R3m$ space group at 0 GPa although several other structures are also possible. At 150 GPa, the $Fm\bar{3}m$ structure is the most probable.

tally observed Cu_3Au-type structure with the $Pm\bar{3}m$ space group as one of the probable structures. This structure can be viewed as introducing one Pd vacancy in each unit cell of rocksalt PdH, and therefore can also be written Pd_3VaH_4, where Va represents a vacancy. At high pressure, we find a low-symmetry $P1$ structure with a complex coordination environment as the most probable structure.

Following this analysis, we examine the stable structures of compositions PdH_n where n is an integer between 2 and 12. The most probable structures identified in the structure search are shown in Fig. 2. These structures consist of Pd-H layers or clusters between which H_2 molecules are located. The atomic coordination features of the low enthalpy structures are characterized by the average radial distribution function (RDF) (Figs. S9 and S10). All structures at zero pressure are characterized by Pd-H and H-H bonding but variable bond distances. Whereas nearest neighbor Pd-H distances remain within 1.7-2.0 Å, the nearest neighbor H-H distances change significantly with composition. For PdH_n when n is less than 2-3, the H-H distances are mainly over 2 Å; however, when n is larger than 2-3, H-H forms a peak at about 0.7-0.8 Å, indicating the formation of H_2 molecules. Pressure also affects the RDF significantly. At 150 GPa, for example, H-H distances span a broad range beyond the conventional covalent H_2 bond length, indicating diverse coordination environments of H at high compressions.

To further characterize the structural features of these Pd hydrides, a topological analysis of the low enthalpy structures was performed (Fig. 3). Each structure is based on a Pd-H framework with the void space occupied by extra H atoms if any, which are mainly present in the form of

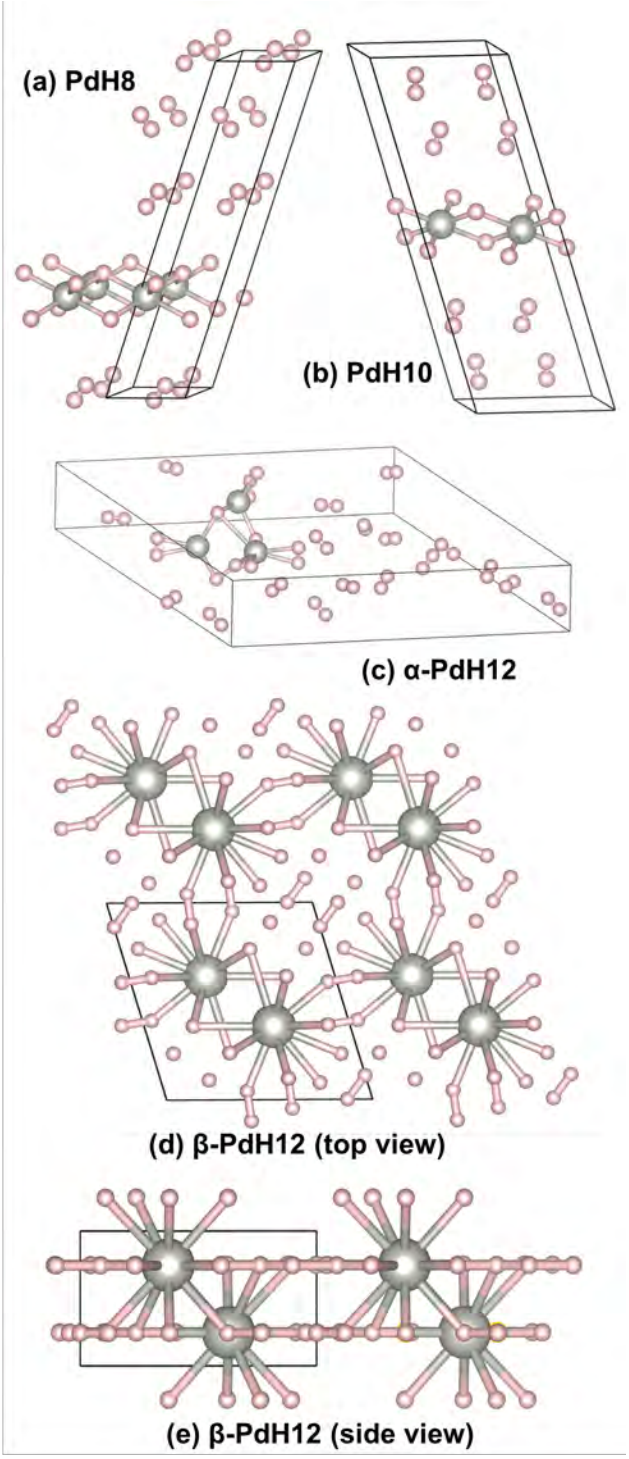

Figure 2: Results of ground-state structure search for (a) PdH_8, (b) PdH_{10}, (c) PdH_{12} at zero pressure and PdH_{12} (d) top and (e) side view at 150 GPa.

H_2 molecules. The basic structural unit in the Pd-H framework is a polyhedron with the Pd atom coordinated by H atoms. The Pd-centered polyhedra can be directly connected with each in terms of sharing of faces, edges or corners, or indirectly connected via intermediate H atoms, forming a network with specific dimensionality. In a 0D framework, the Pd-centered polyhedra are isolated, whereas they can also form columns and layers to give 1D and 2D frameworks, respectively. The network can also extend in three dimensions (3D). Obviously, both pressure and composition have significant influence on the coordination number (CN) of Pd and the dimensionality of the Pd-H framework. At zero pressure, the CN is between 3 and 7, and moderately increases from PdH to PdH_2 but saturates beyond PdH_2, with the maximum CN pinned at 7. The dimensionality also changes around PdH_2 and the transition is even sharper. From PdH to PdH_2, the frameworks are exclusively 3D, whereas beyond PdH_2, no 3D framework is present in the structures examined. From PdH_3 to PdH_6, the frameworks are exclusively 2D, while starting from PdH_7, 1D gradually becomes dominant. At 150 GPa, the frameworks are invariably 3D regardless of the compositions, but CN is diffuse, spanning between 5-18, and shows a dramatic change with composition. Based on the above analysis, it can be concluded that high pressure can compress large amounts of H around Pd and increase the connectivity of the framework components.

The most probable stable structure found for PdH_{12} at 150 GPa is monoclinic with *Cmcm* space group (Fig. 2). This structure is distinct from those predicted as thermodynamically stable phases for rare-earth superhydrides, which are based on clathrate or cage-like structures[8,9]. On the other hand, the structure has similarities to those predicted for MgH_{12} and MgH_{16}, which consists of molecular H_2 units having a range of nearest neighbor distances[17]. The *Cmcm* structure of

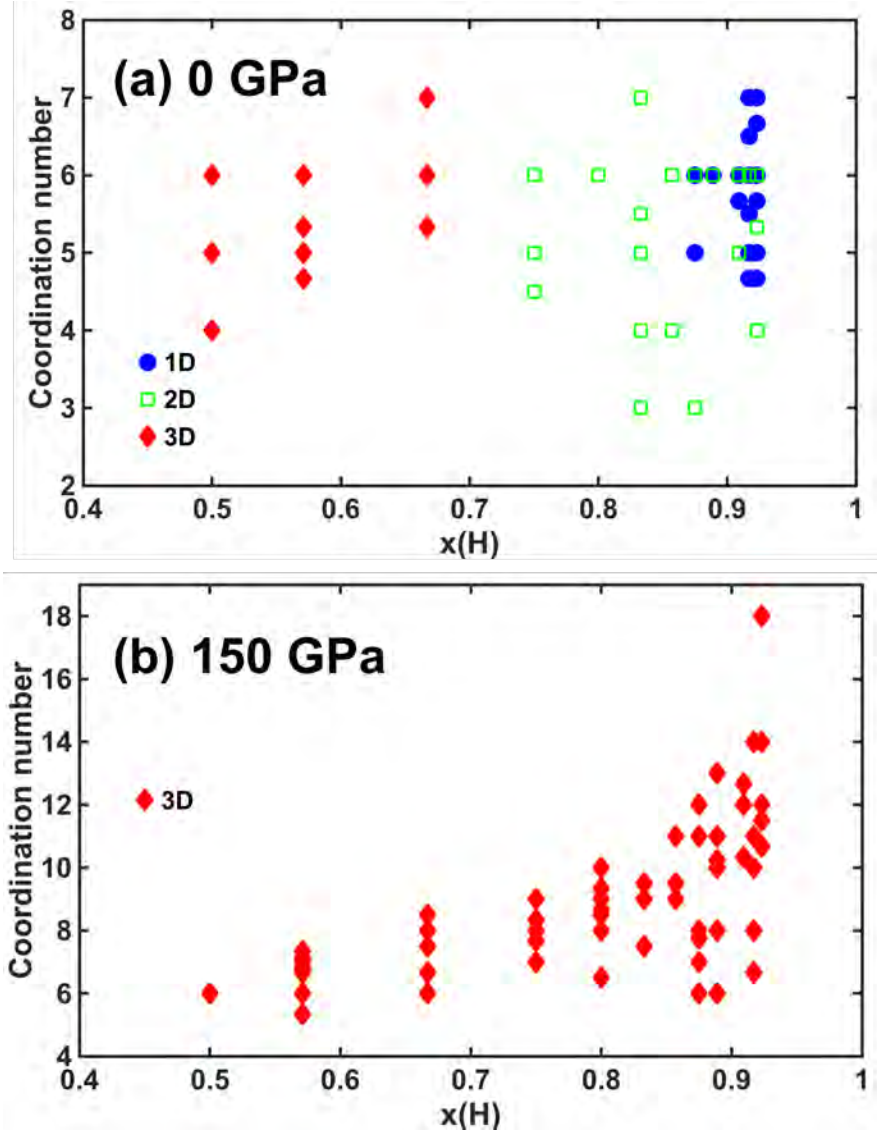

Figure 3: Composition-dependent topological features of the low enthalpy structures at (a) zero pressure and (b) 150 GPa. The coordination number corresponds to the number of nearest neighbor H atoms surrounding a Pd atom, and the dimensionality is used to describe the framework formed by the Pd polyhedra.

PdH_{12} consists of a 3D network of Pd-centered H polyhedrons bridged by H-H covalent bonds with the space in-between filled with H_2 molecules. Interestingly, viewing perpendicular to the monoclinic c axis, all the H atoms are arranged in 2D layers, which are stacked together along the c axis. Fig. 4(a) shows its radial distribution function (RDF). The nearest neighbor Pd-H distances span 1.7-1.9 Å, giving an effective coordination of Pd by H of 14. On the other hand, the H-H distances span a wide range and consist of two groups (1) 0.7-1.0 Å, corresponding to H_2 molecules between polyhedra and the bridging H_2 units that connect polyhedra, and (2) 1.5-2.0 Å, corresponding to neighboring corner H atoms within a polyhedron. The charge density distribution of a (001) plane is plotted in Fig. 4(b). The charge density between H-H is higher than that between Pd-H, indicating that covalent H-H bonds are dominant even under pressures of 150 GPa. This is likely due to zero pressure electronegativities of Pd and H being very close. We conclude that this equivalence persists to high compressions, as evident by the lack of significant charge transfer even under these extreme conditions. Nevertheless, bonding between Pd and H is apparent from the charge density map. The electronic density of states (DOS) is shown in Fig. 4(c), where the total DOS is decomposed to contributions from different orbitals, H-s, Pd-s, Pd-p and Pd-d. The considerable DOS at the Fermi level indicates that the monoclinic PdH_{12} is a metal under these conditions. The dominant partial DOS are from H-s and Pd-d showing strong hybridization, both contributing to conducting electrons.

The H-H distances for the rare-earth superhydrides are in the range of $\sim$1.1 Å at high pressures[8,9]. Recently, evidence for H-H distances below 1.6 Å was found in ZrV_2Hx, even at ambient pressure, from inelastic neutron scattering[18], in violation of the so-called Switendick[19]

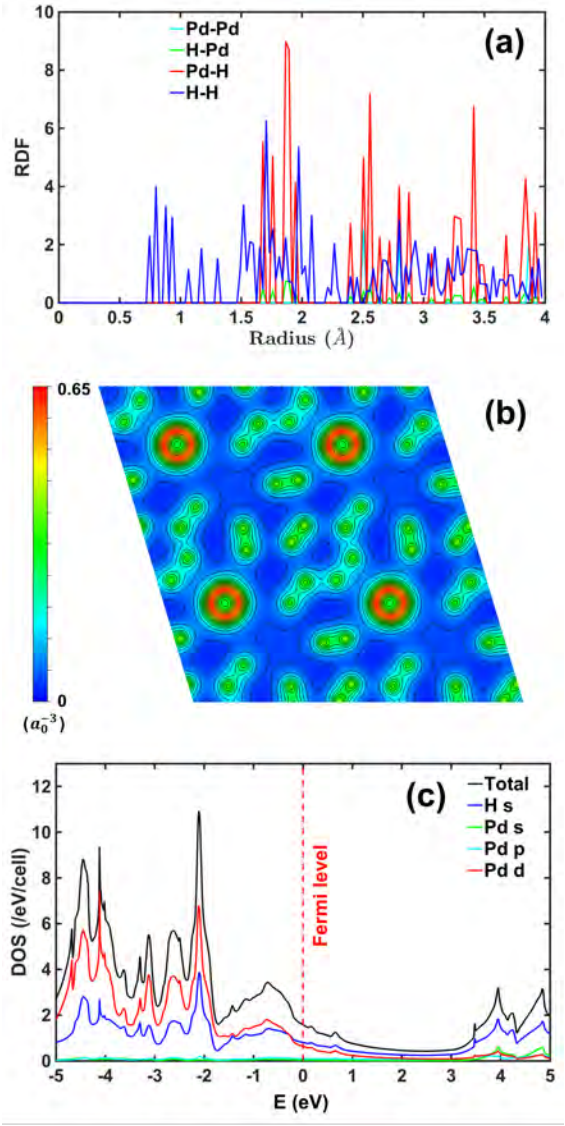

Figure 4: Properties of *Cmcm* PdH_{12} at 150 GPa: (a) Radial distribution function (RDF). The predominant bonding is H-H and Pd-H. Note that the minimum H-H distance is about 0.74 Å, close to H-H bond in molecular H_2. (b) Charge density distribution within the (001) plane. The charge density between H and H is higher than that between Pd and H. The unit of the charge density is a_0^{-3}, where the Bohr radius a_0 = 0.529 Å. The contour lines are spaced by 0.05 a_0^{-3}. (c) Density of states (DOS) and partial density of states (PDOS). The red dashed line is the Fermi level.

criteria for the minimum H-H distances of 2.1 Å in common hydrides. In order to analyze how the H-H distance changes with composition and pressure, the distribution of minimum H-H distances of the low enthalpy structures at both zero pressure and 150 GPa is plotted in Fig. S6. The composition has a large influence on the minimum H-H distance. At zero pressure, the minimum H-H distance is around 2.2-3.1 Å for PdH, but drastically drops to about 0.8 Å for PdH_2, close to the H-H distance in H_2, 0.74 Å. Further increasing H content does not cause significant changes, and the minimum H-H distance is pinned by the H-H distance in H_2 molecule. A similar trend holds for 150 GPa, though the minimum H-H distance usually shrinks compared with that at zero pressure, due to large compression. However, the H-H distance is close to that of free H_2.

Having identified the possible stable structures, we assess the phase stability from an enthalpy convex hull analysis. Using an ensemble of functionals, we generate an ensemble of convex hulls, which are shown in Figs. S7 and S8. Unsurprisingly, We find that no Pd superhydrides are thermodynamically stable at zero pressure. At 150 GPa, there are still no thermodynamically stable superhydrides although PdH_{12} is only slightly unstable, and the stability of superhydrides is greatly increased compared to zero pressure.

Moderate-pressure electrochemical synthesis

Rare-earth superhydrides were first documented experimentally using diamond-anvil cell laser-heating techniques, leading to the discovery of near-room-temperature superconductivity in LaH_{10}[7,20,21]. This result was subsequently confirmed[22], and other metal superhydrides were later observed[23]. We

now discuss a possible alternate approach to synthesizing dense metal superhydrides by combining pressure and electrochemistry. In this approach, an electrode consisting of a metal (or conducting metal hydride) is loaded with hydrogen by holding at an appropriate electrode potential using an electrolyte consisting of mobile protons. The proton-conducting membrane could be an aqueous electrolyte solution, polymer electrolyte membrane (e.g., Nafion)[24], proton-conducting ceramic electrolytes[24], and solid acid proton conductors[25]. The electrolytes provide a way to tune the activity of mobile protons and kinetics of reactions at electrode-electrolyte interfaces.

The hydrogen loading reaction for a metal electrode and an electrolyte containing mobile protons is given by:

$$\mathrm{Pd} + \mathrm{n}(\mathrm{H}^{+} + \mathrm{e}^{-}) \Longleftrightarrow \mathrm{PdH_n} \tag{1}$$

with the associated Gibbs Free Energy of the reaction:

$$\Delta \mathrm{G} = \mathrm{G_{PdH_n}} - \mathrm{G_{Pd}} - \mathrm{nG_{H^+}} - \mathrm{nG_{e^-}}. \tag{2}$$

The free energy of protons at unit activity and electrons at electrode potential zero on the standard hydrogen electrode scale can be related to the free energy of hydrogen gas. Thermodynamic corrections can then be added to account for the effect of electrode potential and activity of protons[26]. The computational hydrogen electrode equation provides the relation, $\mathrm{G_{H^+(a_H^+=1)}} + \mathrm{G_{e^-(U=0)}} = \frac{1}{2}\mathrm{G_{H_2}}$. This provides the relation,

$$\Delta \mathrm{G} = \mathrm{G_{PdH_n}} - \mathrm{G_{Pd}} - \frac{\mathrm{n}}{2}\mathrm{G_{H_2}} + \mathrm{neU_{SHE}} - \mathrm{nk_B T ln}(\mathrm{a_{H^+}}). \tag{3}$$

This relation allows us to construct an electrochemical phase diagram for loading hydrogen into a material as a function of pH and electrode potential. Lowering the electrode potential (making it

more negative) or increasing the activity of protons enables loading higher amounts of hydrogen.

However, in a practical device, at negative potentials, metals tend to catalyze the hydrogen evolution reaction[27], given by,

$$2\mathrm{H}^{+} + 2\mathrm{e}^{-} \Longleftrightarrow \mathrm{H}_2. \tag{4}$$

Hence, electrochemical loading needs to compete with the hydrogen evolution reaction. Electrolyte formulations can suppress the hydrogen evolution reaction kinetically through superconcentrated electrolytes[28] or other suppressing mechanisms. However, we set the limit for electrochemical synthesizability at the potential where reaction free energy for hydrogen evolution on the catalyst surface is thermodynamically downhill, which is determined by the free energy of adsorbed hydrogen on the palladium surface[27].

The electrochemical phase diagram incorporating uncertainty analysis at ambient pressure is shown in Figure 5. At ambient pressure, at $pH = 0,\ (a_{H^+} = 1)$, we find that electrochemical loading of even the PdH phase is challenging and will compete with the hydrogen evolution reaction, as observed experimentally[24]. As Pd catalyzes hydrogen evolution with almost no overpotential[27], thus suppressing hydrogen evolution is the only approach to accessing these phases at ambient conditions. Further, it is likely that the bulk loading reaction will have slower kinetics than surface catalyzed hydrogen evolution reaction making this even more challenging. Next, we explore the effect of very high pressures, and find that it is possible to produce PdH_{12} below the hydrogen evolution potentials.

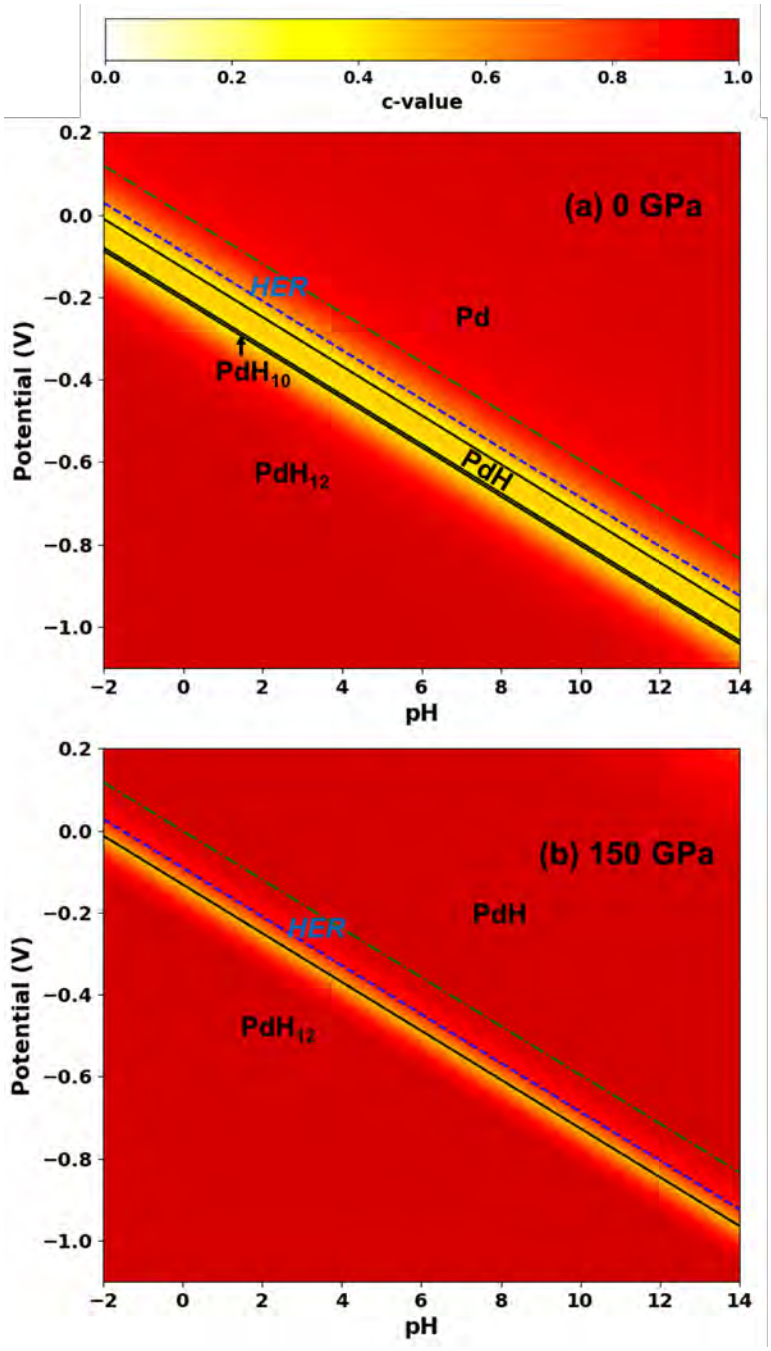

Figure 5: Pourbaix diagram by BEEF-vdW ensmebles at (a) zero pressure and (b) 150 GPa. The solid black lines are phase boundaries calculated by the best-fit BEEF functional. The dotted dashed green line represents the equilibrium HER (hydrogen evoluation reaction) on Pd, while the blue dashed line takes overpotential into consideration.

The above analysis raises the intriguing question of whether such palladium superhydrides could be synthesized at modest pressures, e.g., at 100 MPa (kilobar) versus 100 GPa (megabar) conditions. Although electrochemical studies have been performed over the years in the 100 MPa range (maximum of 1 GPa[29]), the field remains largely unexplored. To examine the possibility to stablize Pd superhydrides at modest pressures, we calculate a comprehensive pressure dependent Pourbaix diagram at 300 K, with the reversible hydrogen electrode (RHE) as the reference (Fig. 6). At decreasing potentials, the phase transition sequence is Pd $\rightarrow$ PdH $\rightarrow$ PdH_{10} $\rightarrow$ PdH_{12}. The most thermodynamically accessible Pd superhydride, PdH_{10} has a very narrow potential window near ambient pressure, which is gradually enlarged with increasing pressure. The phase boundary between PdH and PdH_{10}, can be fitted as the following relation:

$$U = -0.168 + 0.0297 * \log_{10}(P) + 8.83 * 10^{-5} \times P^{2/3}, \quad (5)$$

where U is the electrode potential on the RHE scale (in V) needed to transform PdH to PdH_{10} under a given pressure P (in MPa). The above relation has good linearity between U and logP near the ambient pressure. The power of the electrochemical driving force is illustrated by the fact that an order of magnitude reduction of the transition pressure can be achieved by only 0.03 V change in the electrode potential. When the pressure approaches 10^3 MPa (1 GPa), non-linearity of the relation becomes significant. The superhydride PdH_{10} can be stablized at about 200 MPa (0.2 GPa) at the onset potential for hydrogen evolution. Using superconcentrated electrolytes that can suppress HER further, it is expected that PdH_{10} can be stablized under even lower pressure operating at a more negative potential.

Finally, from an electrochemical synthesis standpoint, palladium is among the most difficult

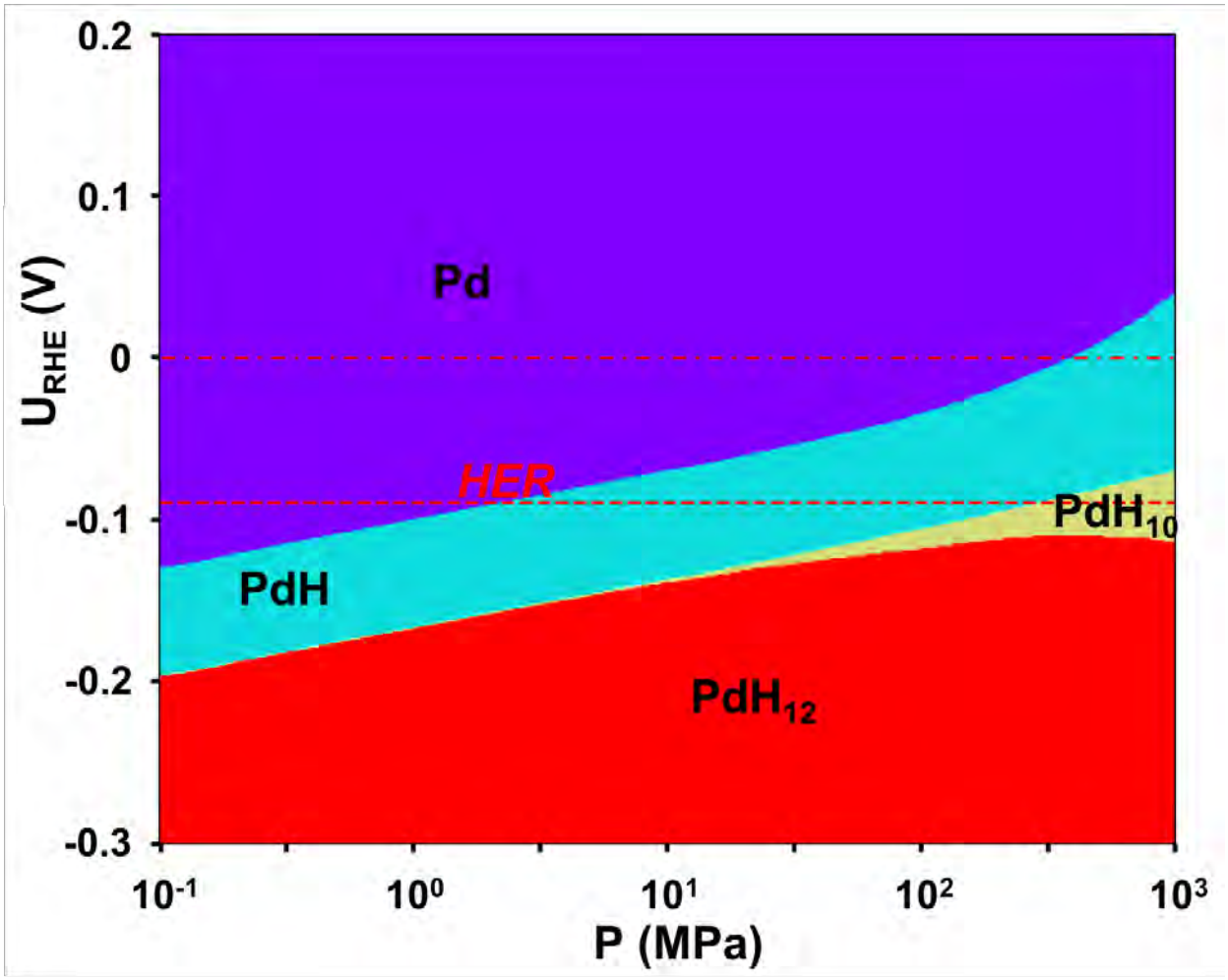

Figure 6: Pressure dependent Pourbaix diagram by the best-fit BEEF-vdW functional at 300 K. The dotted dashed red line represents the equilibrium HER (hydrogen evolution reaction) on Pd, while the red dashed line takes overpotential into consideration.

as it catalyzes hydrogen evolution with negligible overpoential.[27] Thus, we expect that this similar strategy is likely to work and probably at lower pressures for other metal superhydrides.

Conclusion

Using first-principles density functional theory calculations and particle swarm structure search, the phase stability of superhydrides of palladium have been studied. From an analysis of the electrochemical loading of hydrogen in Pd under a broad range of pressures, remarkably we find that PdH_{10} can be electrochemically synthesized before the onset of hydrogen evolution at even modest pressures of 200 MPa, which is readily accessible using existing high pressure methods. Given that palladium is among the most active metals for hydrogen evolution, we believe that it will be even easier to synthesize other metal superhydrides. Combining pressure and electrode potential thus offers an alternate route to synthesize metal superhydrides and other novel materials at currently accessible static pressure conditions, and a framework for such synthesis has been provided. Numerous extensions of existing electrochemical and high pressure techniques could lead altogether new materials created under an even broader range of pressures. This work should serve to open up the new frontier of high-pressure electrochemistry to produce exciting new materials with broad applications[5,30].

Methods

Calculation Details: All BEEF-vdW calculation were run using a real space grid implementation of the projector augmented wave approximation through the GPAW software [31–33]. A real space

grid with spacing of 0.16 Å is used for the representation of electronic wavefunctions, and a k-point density of larger than 30 Å in reciprocal space was used in each dimension. For each material, the geometry is relaxed to a maximum force of less than 0.01 eV/Å.

Structure Search: The particle swarm optimization is employed for structure search, using the CALYPSO code[10,11]. Since only the superhydrides are of interests here, the compositions PdH_n (n is an integer and $1 \leq n \leq 12$) and Pd_3H_4 which is the highest Pd hydride reported in experiments so far, totaling 13 compositions in all. For each composition, one unit cell is allowed to have 1-4 formulas. For a fixed number of formula at a given composition, about 1000 structures were searched during the structure evolution.

Bayesian Error Estimation Funtional: For each material, a collection of functionals at the level of the generalized gradient approximation (GGA) were used as described below. For the purpose of error estimation, the Bayesian error estimation functional with van der Waals correction [34] was used. Besides acting in the usual manner for the self consistent calculation of the exchange correlation energy, this empirically fit functional can generate an ensemble of functionals that are small perturbations away from the main functional fit in exchange correlation space.

The exchange-correlation energy for the BEEF-vdW is given in Ref. 34 as

$$E_{xc} = \sum_m a_m \int \varepsilon_x^{UEG}(n) B_m[t(s)] d\mathbf{r} + \alpha_c E^{LDA-c} + (1-\alpha_c) E^{PBE-c} + E^{nl-c}. \quad (6)$$

Here B_m is the mth Legendre basis function, each of which has a corresponding expansion coefficient a_m. The expansion coefficients, as well as the α_c parameter that mixes the local density approximation (LDA) and PBE[35] exchange correlation functionals, have been pre-fit with respect

to a range of data sets as described in Ref. 34. Additionally within the functional is the E^{nl-c} non-local correlation term implemented via the vdW-DF2[36] method. The method to generate the ensemble of functionals was tuned such that the spread of the predictions of the functionals matches the error of the main self consistent functional with respect to the training and experimental data on which it was originally trained. Each of these functionals can then provide a non self consistent prediction of energy and therefore allows for a computationally efficient yet systematic way of understanding the sensitivity of the final prediction with respect to small changes in exchange correlation functional.

Confidence-value (c-value) Calculations: We use the confidence value (c-value)[12], for determining the uncertainty associated with the choice of the functional. We define c-value to be the fraction of the ensemble that predict a certain structure to be the ground state. For a fixed composition, this simply involves counting the fraction of functionals that predict a particular structure to be the ground state. This framework can be expanded to construct a c-value associated with a Pourbaix diagram. In this case, the c(U, pH), for a specific phase is defined as the fraction of functionals that predict it to have the lowest free energy at a given potential and pH, given by

$$c_i(U, pH) = \frac{1}{N_{ens}} \sum_{n=1}^{N_{ens}} \prod_{j \neq i} \Theta(\Delta G_j^n(U, pH) - \Delta G_i^n(U, pH)) \tag{7}$$

where the summation is over number of ensembles, $N_{ens} = 2000$ here, and the product is over all the remaining possible phases. $\Theta(x)$ denotes the Heaviside step function. At any given U and pH, $i, j \in S$, the set of all considered phases.

Topological analysis: The coordination number is determined using the CrystalNN class based on a Voronoi algorithm in pymatgen[37]. The framework of the crystal structure and its dimensionality are identified using the Zeo++ code based on the Voronoi decomposition[38], where radii of 0.5 Å and 1.6 Å are adopted for H and Pd respectively.

Acknowledgements This work was partially supported by Google and by the DOE/NNSA and NSF-DMR (R.J.H.). The Authors would like to thank helpful discussions with Yet-Ming Chiang, Matt Trevithick and Florian Metzler.

Contributions P.G. and V.V. conceived the idea for the project, and R.J.H. provided input on the high pressure calculations and experiments. P.G. ran all the DFT calculations. All authors discussed the results and jointly wrote the manuscript.

Competing Interests V.V. and P.G. are inventors on a provisional patent application, 63/028,265 related to electrochemical synthesis of metal superhydrides.

Correspondence Correspondence and requests for materials should be addressed to V. Viswanathan (email: venkvis@cmu.edu) and R.J.Hemley (rhemley@uic.edu).

Additional information Supplementary Information attached and consists of Supplementary Figures 1-11.

1. Flanagan, T. B. & Oates, W. The palladium-hydrogen system. *Annual Review of Materials Science* **21**, 269–304 (1991).

2. Viswanathan, B., Sastry, M. V. C. & Murthy, S. S. *Metal hydrides: fundamentals and applications* (Springer, 1998).

3. Skoskiewicz, T. Superconductivity in the palladium-hydrogen and palladium-nickel-hydrogen systems. *Physica Status Solidi (a)* **11**, K123–K126 (1972).

4. Boudart, M. & Hwang, H. Solubility of hydrogen in small particles of palladium. *Journal of catalysis* **39**, 44–52 (1975).

5. Berlinguette, C. P. *et al.* Revisiting the cold case of cold fusion. *Nature* **570**, 45–51 (2019).

6. Fukai, Y. & Ōkuma, N. Formation of superabundant vacancies in pd hydride under high hydrogen pressures. *Physical review letters* **73**, 1640 (1994).

7. Geballe, Z. M. *et al.* Synthesis and stability of lanthanum superhydrides. *Angewandte Chemie International Edition* **57**, 688–692 (2018).

8. Liu, H., Naumov, I. I., Hoffmann, R., Ashcroft, N. & Hemley, R. J. Potential high-tc superconducting lanthanum and yttrium hydrides at high pressure. *Proceedings of the National Academy of Sciences* **114**, 6990–6995 (2017).

9. Peng, F. *et al.* Hydrogen clathrate structures in rare earth hydrides at high pressures: possible route to room-temperature superconductivity. *Phys. Rev. Lett.* **119**, 107001 (2017).

10. Wang, Y., Lv, J., Zhu, L. & Ma, Y. Crystal structure prediction via particle-swarm optimization. *Physical Review B - Condensed Matter and Materials Physics* **82**, 094116 (2010). 1008.3601.

11. Wang, Y., Lv, J., Zhu, L. & Ma, Y. CALYPSO: A method for crystal structure prediction. *Computer Physics Communications* **183**, 2063–2070 (2012).

12. Houchins, G. & Viswanathan, V. Quantifying confidence in density functional theory predictions of magnetic ground states. *Physical Review B* **96** (2017). URL https://doi.org/10.1103/physrevb.96.134426.

13. Guan, P. W., Houchins, G. & Viswanathan, V. Uncertainty quantification of DFT-predicted finite temperature thermodynamic properties within the Debye model. *Journal of Chemical Physics* **151**, 244702 (2019). URL http://aip.scitation.org/doi/10.1063/1.5132332. 1910.07891.

14. Houchins, G. & Viswanathan, V. Towards ultra low cobalt cathodes: A high fidelity computational phase search of layered li-ni-mn-co oxides. *Journal of The Electrochemical Society* **167**, 070506 (2020). URL https://doi.org/10.1149/2.0062007jes.

15. Brownsberger, K. *et al.* X-ray diffraction, lattice structure, and equation of state of pdh x and pdd x to megabar pressures. *The Journal of Physical Chemistry C* **121**, 27327–27331 (2017).

16. Guigue, B., Geneste, G., Leridon, B. & Loubeyre, P. An x-ray study of palladium hydrides up to 100 gpa: Synthesis and isotopic effects. *Journal of Applied Physics* **127**, 075901 (2020).

17. Lonie, D. C., Hooper, J., Altintas, B. & Zurek, E. Metallization of magnesium polyhydrides under pressure. *Phys. Rev. B* **87**, 054107 (2013).

18. Borgschulte, A. *et al.* Inelastic neutron scattering evidence for anomalous h–h distances in metal hydrides. *Proceedings of the National Academy of Sciences* **117**, 4021–4026 (2020).

19. Switendick, A. Band structure calculations for metal hydrogen systems. *Z. Phys. Chem.* **117**, 89–112 (1979).

20. Somayazulu, M. *et al.* Evidence for superconductivity above 260 k in lanthanum superhydride at megabar pressures. *Phys. Rev. Lett.* **122**, 027001 (2019). URL https://link.aps.org/doi/10.1103/PhysRevLett.122.027001.

21. Hemley, R. J., Ahart, M., Liu, H. & Somayazulu, M. Road to room-temperature superconductivity: Tc above 260 k in lanthanum superhydride under pressure (2019). 1906.03462.

22. Drozdov, A. P. *et al.* Superconductivity at 250 K in lanthanum hydride under high pressures. *Nature* **569**, 528–531 (2019). URL https://doi.org/10.1038/s41586-019-1201-8. 1812.01561.

23. Zurek, E. & Bi, T. High-temperature superconductivity in alkaline and rare earth polyhydrides at high pressure: A theoretical perspective (2019). URL https://doi.org/10.1063/1.5079225. 1810.12338.

24. Benck, J. D., Jackson, A., Young, D., Rettenwander, D. & Chiang, Y.-M. Producing high concentrations of hydrogen in palladium via electrochemical insertion from aqueous and solid electrolytes. *Chemistry of Materials* **31**, 4234–4245 (2019).

25. Haile, S. M., Chisholm, C. R., Sasaki, K., Boysen, D. A. & Uda, T. Solid acid proton conductors: from laboratory curiosities to fuel cell electrolytes. *Faraday discussions* **134**, 17–39 (2007).

26. Nørskov, J. K. *et al.* Origin of the overpotential for oxygen reduction at a fuel-cell cathode. *The Journal of Physical Chemistry B* **108**, 17886–17892 (2004).

27. Nørskov, J. K. *et al.* Trends in the exchange current for hydrogen evolution. *Journal of The Electrochemical Society* **152**, J23–J26 (2005).

28. Suo, L. *et al.* water-in-salt electrolyte enables high-voltage aqueous lithium-ion chemistries. *Science* **350**, 938–943 (2015).

29. Cruanes, M. T., Drickamer, H. G. & Faulkner, L. R. Electrochemical measurements at high pressure: solvation and the thermodynamics of electron-transfer reactions. *The Journal of Physical Chemistry* **96**, 9888–9892 (1992). URL https://doi.org/10.1021/j100203a057. https://doi.org/10.1021/j100203a057.

30. Flores-Livas, J. A. *et al.* A perspective on conventional high-temperature superconductors at high pressure: Methods and materials. *Physics Reports* **856**, 1–78 (2020). URL https://doi.org/10.1016/j.physrep.2020.02.003.

31. Mortensen, J. J., Hansen, L. B. & Jacobsen, K. W. Real-space grid implementation of the projector augmented wave method. *Phys. Rev. B* **71**, 035109 (2005). URL https://link.aps.org/doi/10.1103/PhysRevB.71.035109.

32. Enkovaara, J. *et al.* Electronic structure calculations with GPAW: a real-space implementation of the projector augmented-wave method. *J. Phys. Condens. Matter* **22**, 253202 (2010). URL https://doi.org/10.1088%2F0953-8984%2F22%2F25%2F253202.

33. Larsen, A. H. *et al.* The atomic simulation environment—a python library for working with atoms. *J. Phys. Condens. Matter* **29**, 273002 (2017). URL http://stacks.iop.org/0953-8984/29/i=27/a=273002.

34. Wellendorff, J. *et al.* Density functionals for surface science: Exchange-correlation model development with bayesian error estimation. *Phys. Rev. B* **85**, 235149 (2012).

35. Perdew, J. P., Burke, K. & Ernzerhof, M. Generalized gradient approximation made simple. *Phys. Rev. Lett.* **77**, 3865–3868 (1996). URL https://link.aps.org/doi/10.1103/PhysRevLett.77.3865.

36. Lee, K., Murray, É. D., Kong, L., Lundqvist, B. I. & Langreth, D. C. Higher-accuracy van der waals density functional. *Physical Review B* **82**, 081101 (2010).

37. Ong, S. P. *et al.* Python Materials Genomics (pymatgen): A robust, open-source python library for materials analysis. *Computational Materials Science* **68**, 314–319 (2013).

38. Willems, T. F., Rycroft, C. H., Kazi, M., Meza, J. C. & Haranczyk, M. Algorithms and tools for high-throughput geometry-based analysis of crystalline porous materials. *Microporous and Mesoporous Materials* **149**, 134–141 (2012).

Supplementary Information: Combining pressure and electrochemistry to synthesize palladium superhydrides

Pin-Wen Guan[1], Russell J. Hemley[2,3], Venkatasubramanian Viswanathan[1,4]

[1]*Department of Mechanical Engineering, Carnegie Mellon University, Pittsburgh, Pennsylvania 15213, USA*

[2]*Department of Physics, University of Illinois at Chicago, Chicago, IL 60607 USA*

[3]*Department of Chemistry, University of Illinois at Chicago, Chicago, IL 60607 USA*

[4]*Department of Physics, Carnegie Mellon University, Pittsburgh, Pennsylvania 15213, USA*

This PDF includes:

Supplementary Figures 1-11.

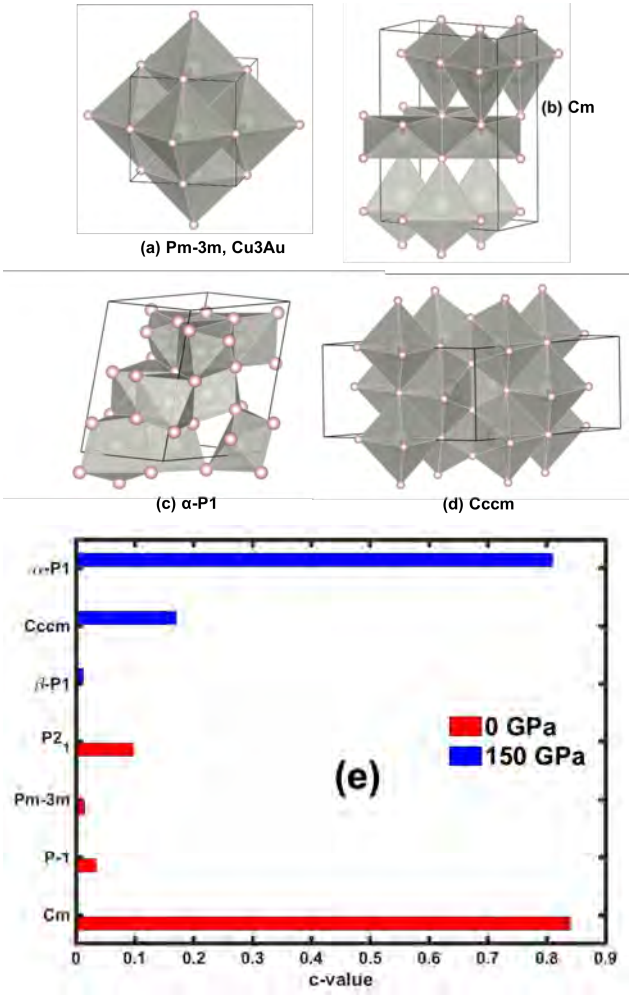

Supplementary Figure 1: Crystal structures of Pd_3H_4: (a) $Pm\bar{3}m$ (b) Cm and (c) $\alpha - P1$ (d) $Cccm$. In the $Pm\bar{3}m$ structure, the Pd atom is octahedrally coordinated, whereas in the Cm structure, the Pd atom has two different coordinations, with 5 and 6 neighboring H atoms respectively. The Pd atom in the low-symmetry $\alpha - P1$ structure has on average 7.11 neighboring H atoms. (d) c-values of Pd_3H_4 at 0 GPa and 150 GPa calculated by BEEF. The most probable structure has the Cm space group, with $Pm\bar{3}m$ among the probable structures. At 150 GPa, $\alpha - P1$ structure is calculated to be the most probable.

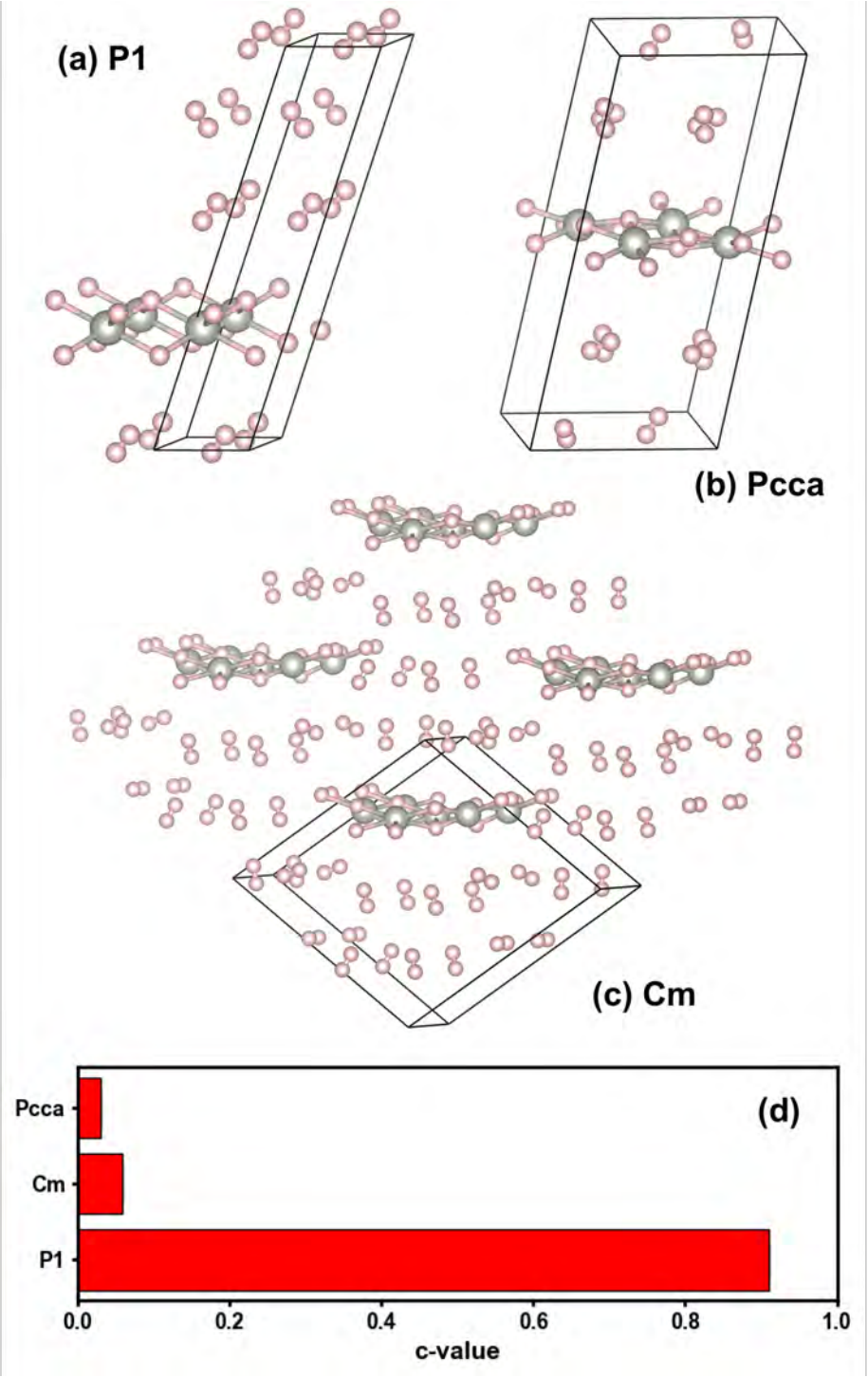

Supplementary Figure 2: Crystal structures of probable ground states of PdH8 at 0 GPa: (a) $P1$ (b) $Pcca$ (c) Cm. (d) Ground states with c-values of PdH_8 at 0 GPa calculated by BEEF. The most probable structure has the $P1$ space group.

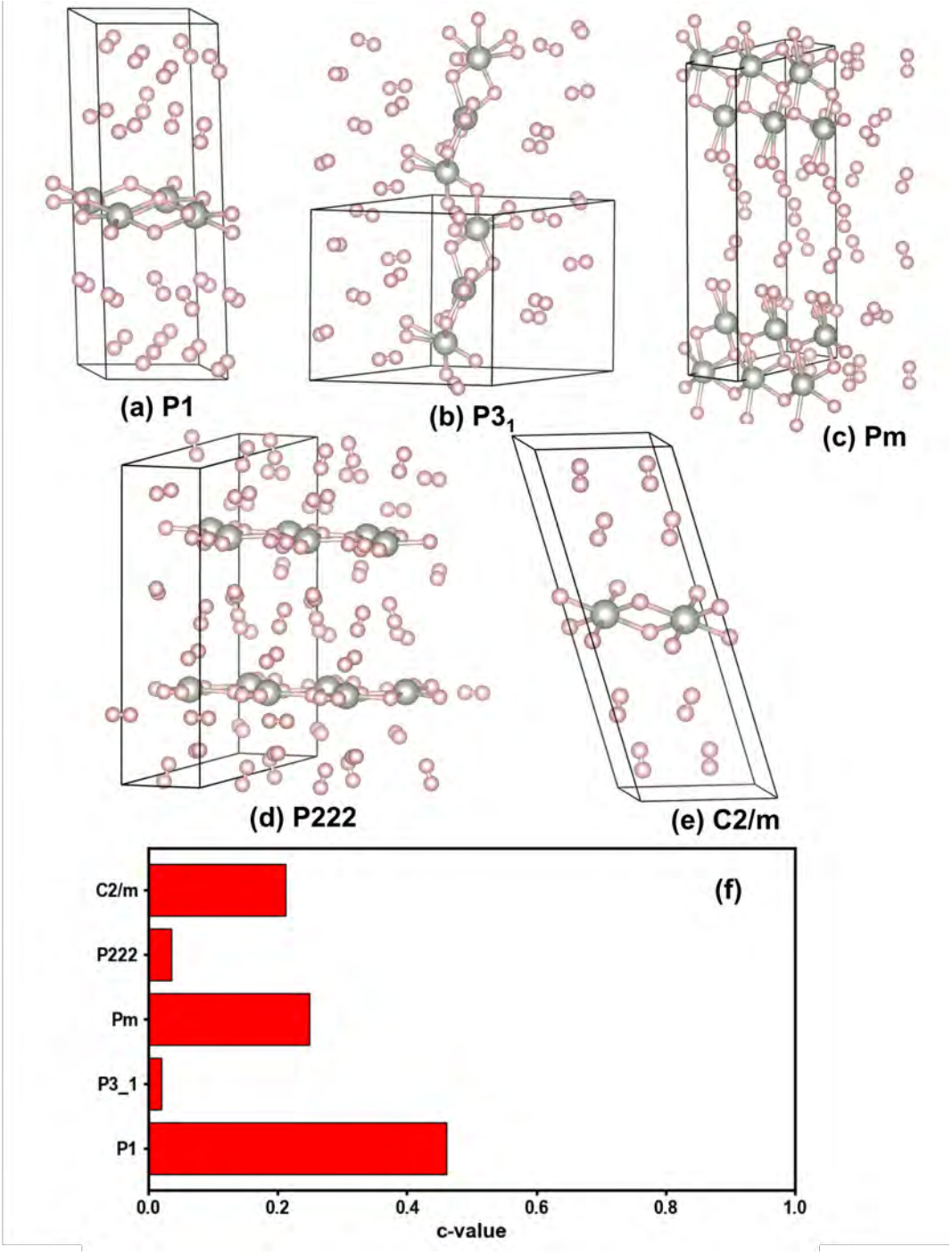

Supplementary Figure 3: Crystal structures of probable ground states of PdH10 at 0 GPa: (a) $P1$ (b) $P3_1$ (c) Pm (d) $P222$ (e) $C2/m$. (f) Ground states with c-values of PdH_{10} at 0 GPa calculated by BEEF. The most probable structure has the $P1$ space group.

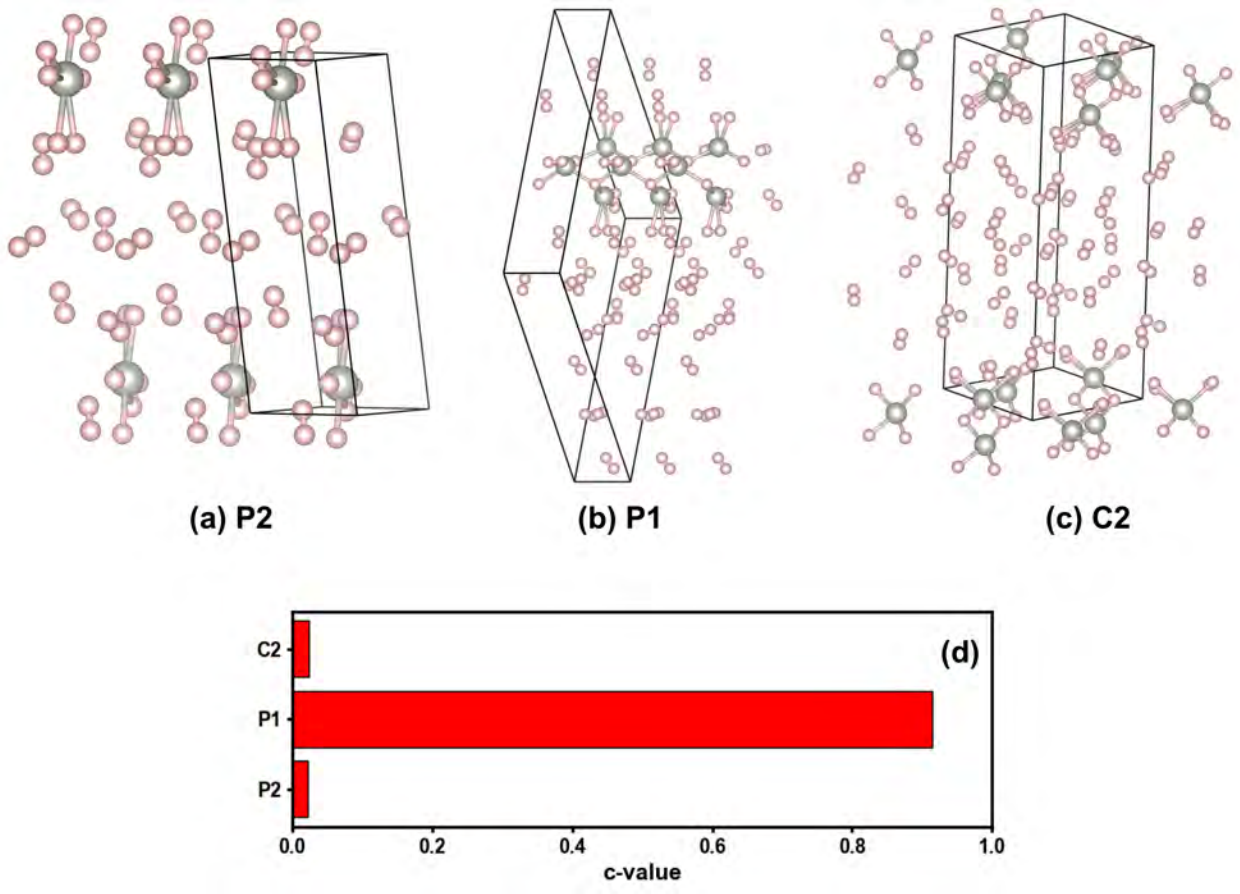

Supplementary Figure 4: Crystal structures of probable ground states of PdH12 at 0 GPa: (a) $P2$ (b) $P1$ (c) $C2$. (d) Ground states with c-values of PdH_{12} at 0 GPa calculated by BEEF. The most probable structure has the $P1$ space group.

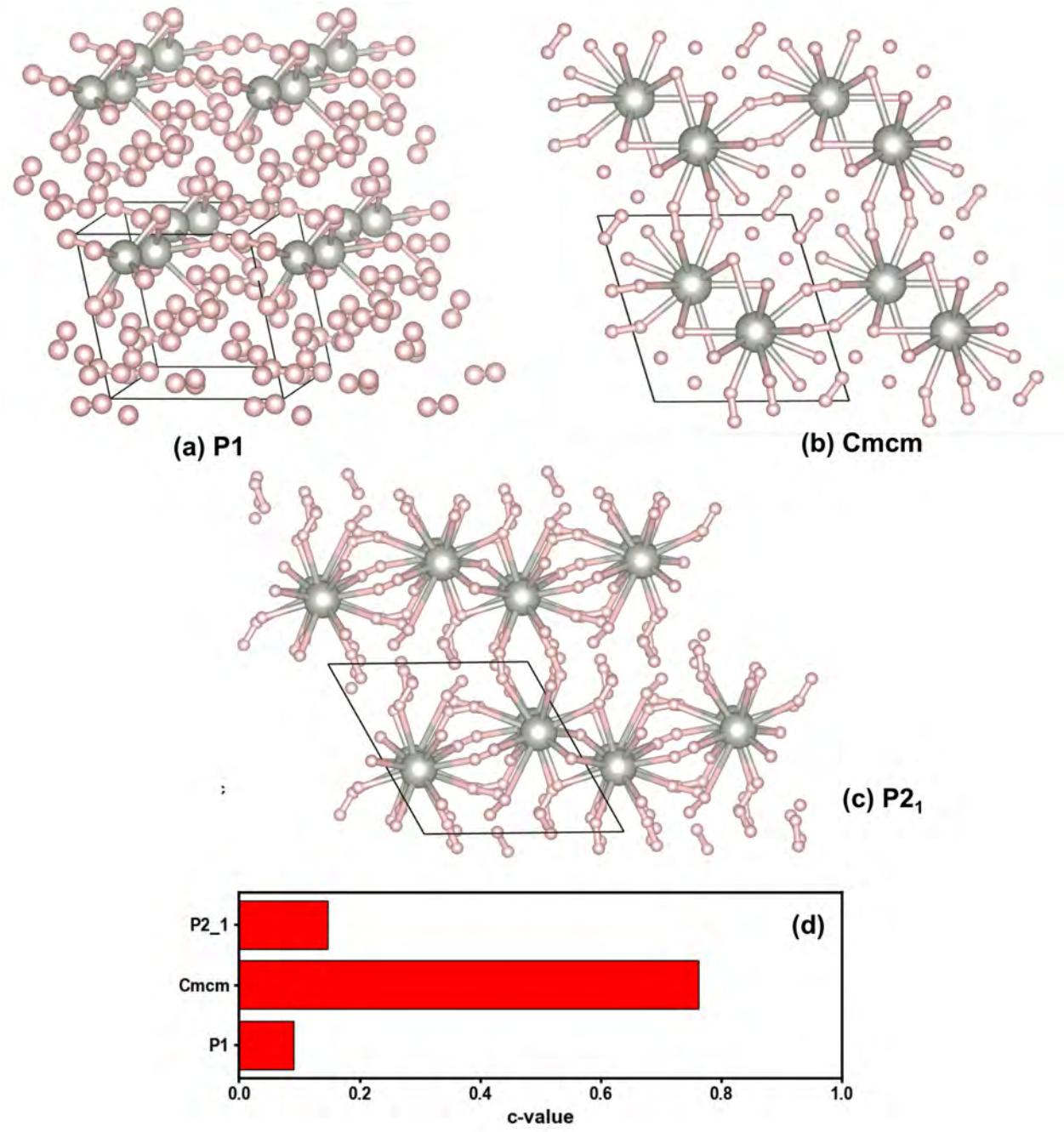

Supplementary Figure 5: Crystal structures of probable ground states of PdH12 at 150 GPa: (a) P1 (b) Cmcm (c) $P2_1$. (d) Ground states with c-values of PdH_{12} at 150 GPa calculated by BEEF. The most probable structure has the Cmcm space group.

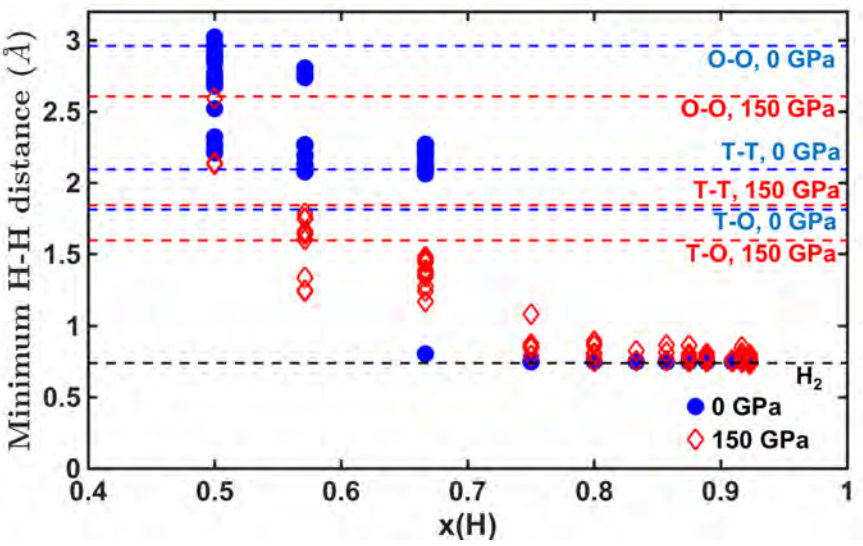

Supplementary Figure 6: Distribution of the minimum H-H distances of the low enthalpy structures at zero pressure and 150 GPa. The black dashed line represents the H-H distance in H_2 (0.74 Å).

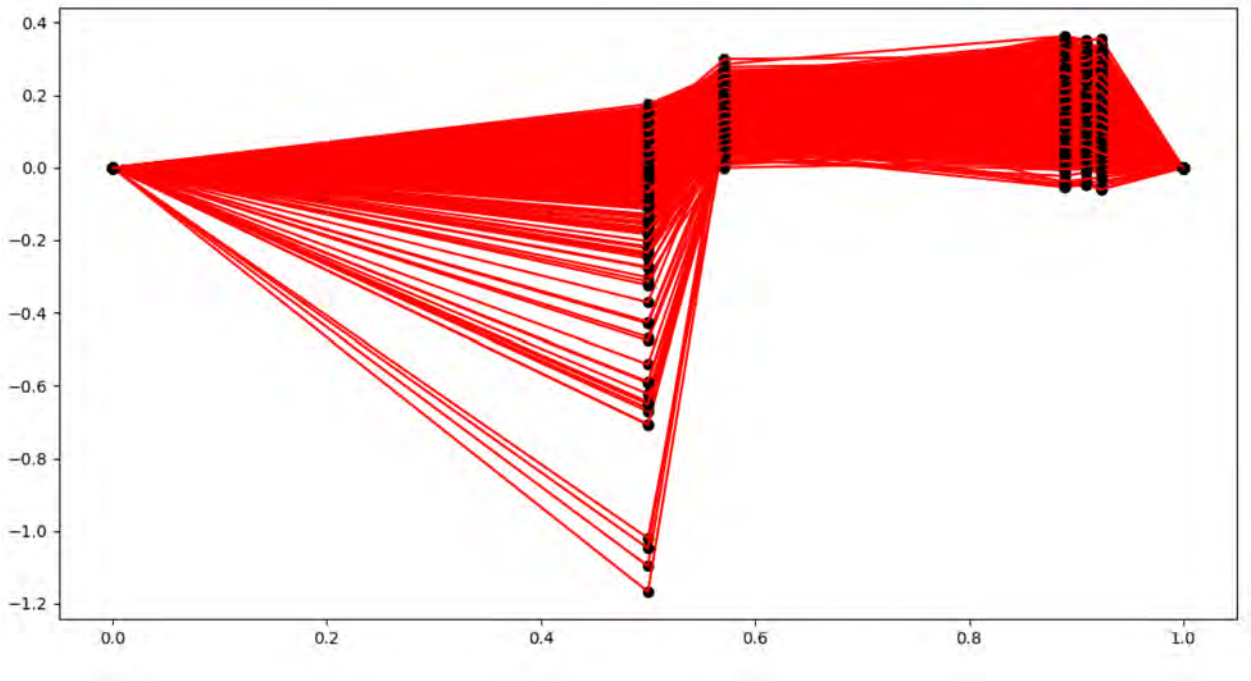

Supplementary Figure 7: Enthalpy convex hull of Pd-H at 0 GPa by BEEF, consisting of results from 2000 different functionals. For most functionals, Pd superhydrides are unstable against PdH and H_2.

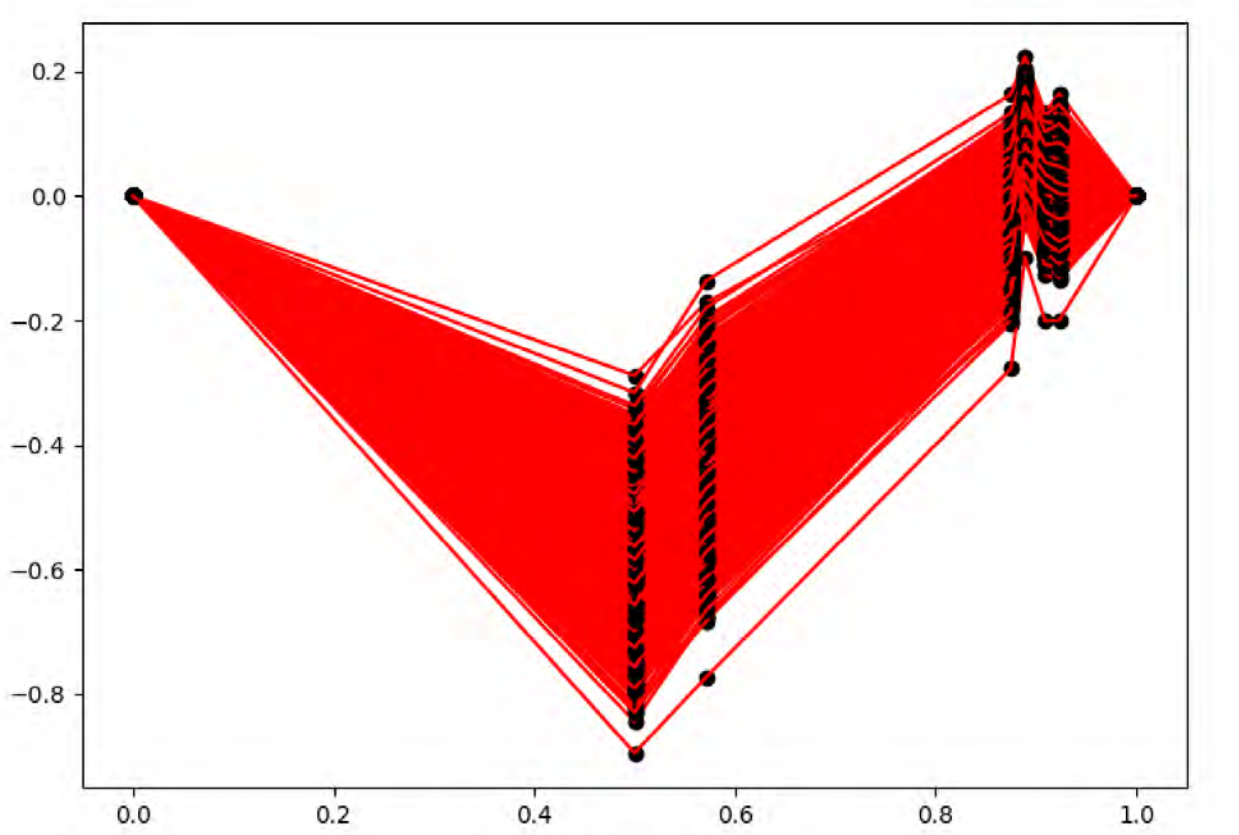

Supplementary Figure 8: Enthalpy convex hull of Pd-H at 150 GPa by BEEF, consisting of results from 2000 different functionals. For most functionals, Pd superhydrides are unstable against PdH and H_2.

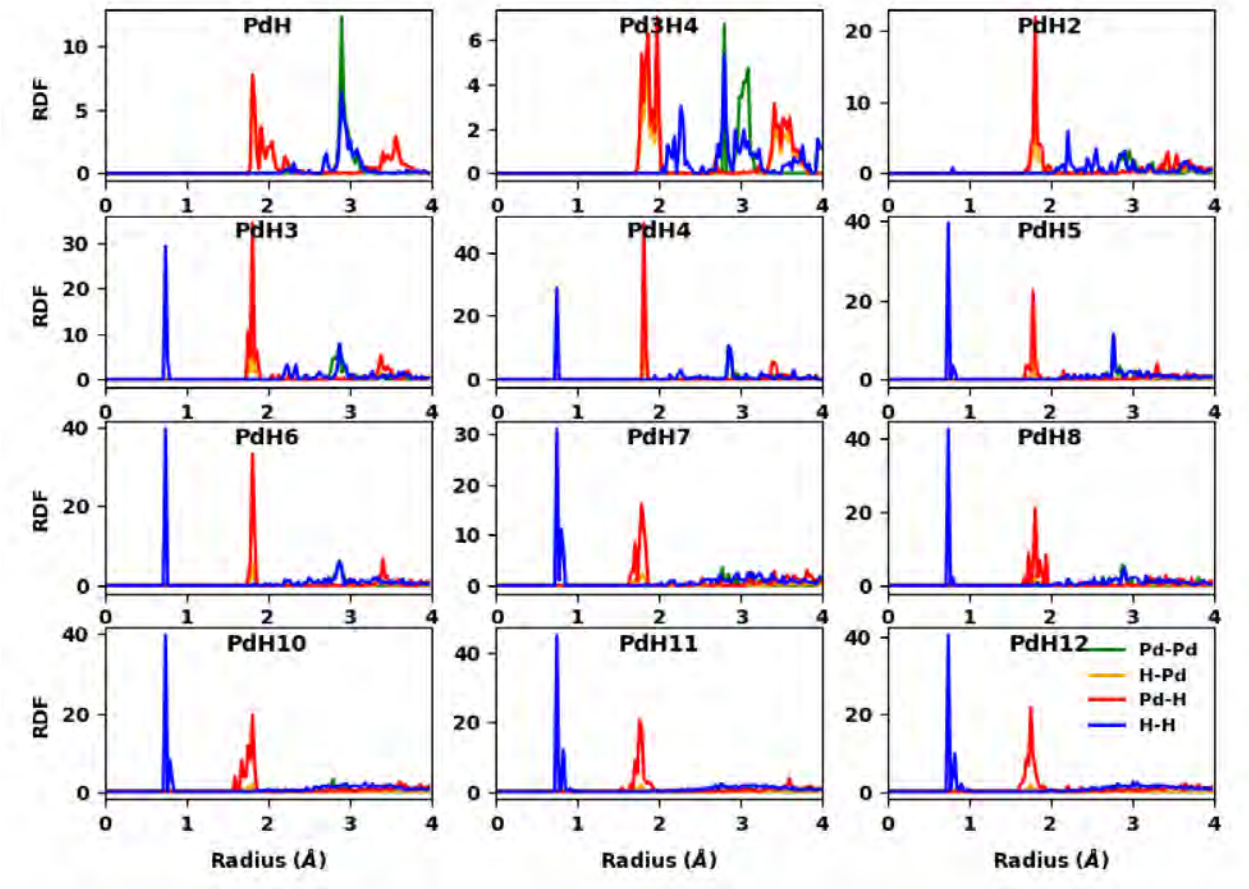

Supplementary Figure 9: Radial Distribution Function (RDF) of low enthalpy structures of PdHn under 0 GPa.

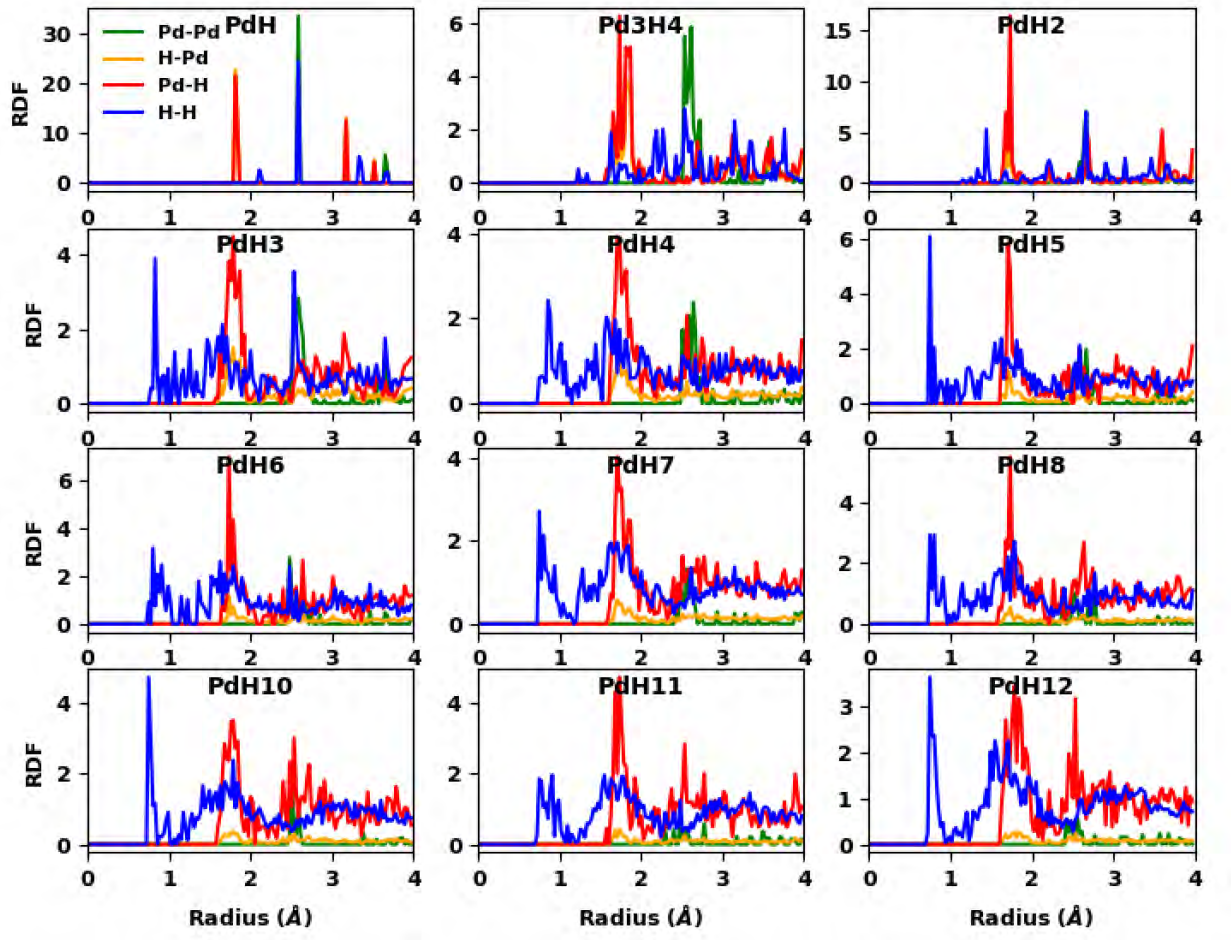

Supplementary Figure 10: Radial Distribution Function (RDF) of low enthalpy structures of PdHn under 150 GPa.

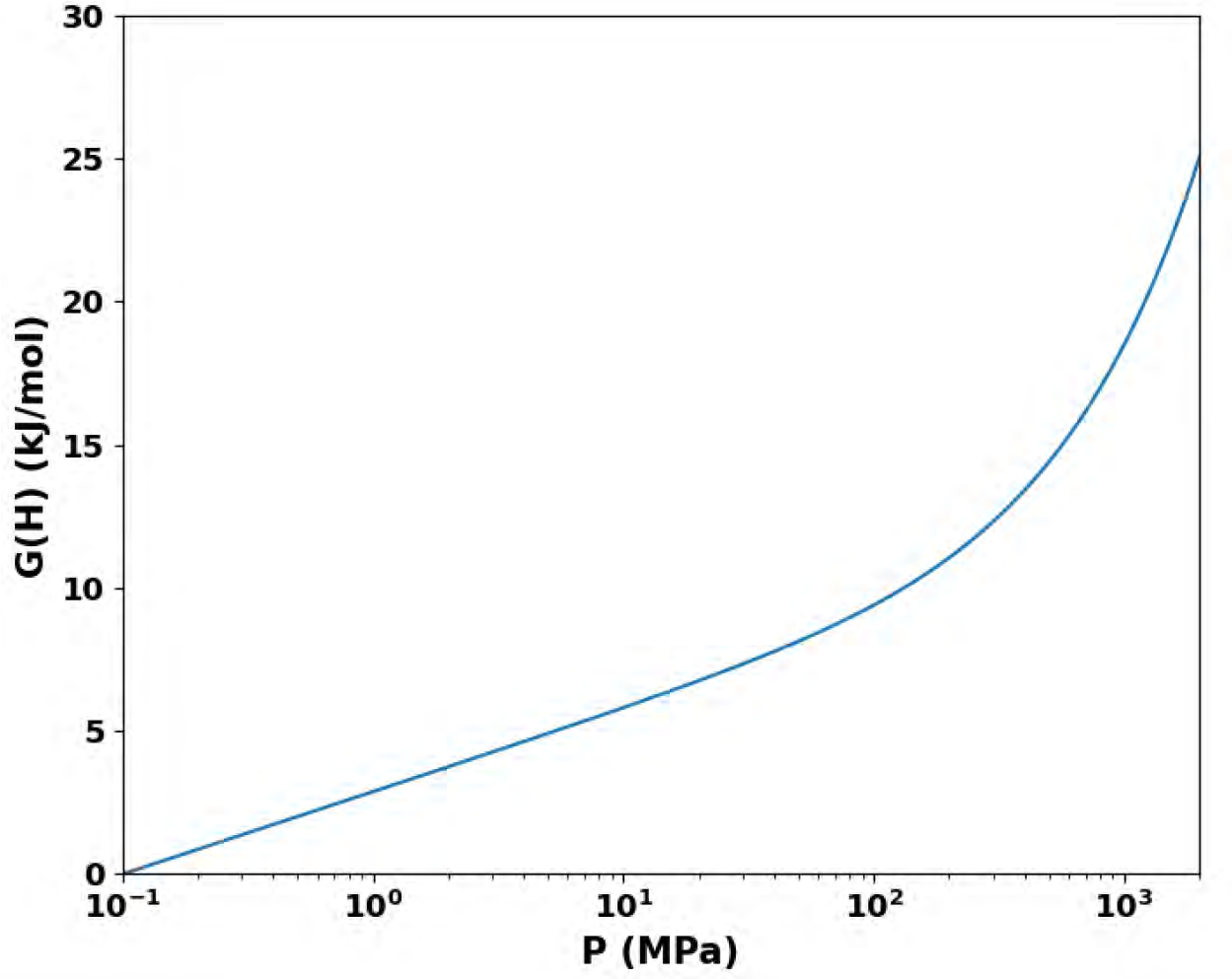

Supplementary Figure 11: Molar Gibbs energy of H as a function of pressure at 300 K, with its value under 1 atm (0.1 MPa) as the reference.